Article

Development of Raman Lidar for Remote Sensing of CO_2 Leakage at an Artificial Carbon Capture and Storage Site

Daewon Kim [1], Hyeongwoo Kang [1], Jea-Yong Ryu [2], Seong-Chun Jun [3], Seong-Taek Yun [4], SungChul Choi [5], SunHo Park [5], MoonSang Yoon [5] and Hanlim Lee [1,*]

[1] Division of Earth Environmental System Science Major of Spatial Information Engineering, Pukyong National University, Busan 48513, Korea; k.daewon91@gmail.com (D.K.); rkdguddn202@gmail.com (H.K.)
[2] Department of Urban Environmental Engineering, Kyungnam University, Gyeongsangnam-do 631-701, Korea; jaeyong03@gmail.com
[3] GeoGreen21 Co., Ltd., Seoul 08376, Korea; sc-jun@daum.net
[4] Department of Earth and Environmental Sciences, Korea University, Seoul 02841, Korea; styun@korea.ac.kr
[5] SOLETOP Co., Ltd., 409 Expo-ro, Yuseong-gu, Daejeon 34051, Korea; lidarchoi@hanmail.net (S.C.); deniro023@naver.com (S.P.); darsang@nate.com (M.Y.)
* Correspondence: hllee@pknu.ac.kr; Tel.: +82-51-629-6688

check for updates

Abstract: We developed a Raman lidar system that can remotely detect CO_2 leakage and its volume mixing ratio (VMR). The system consists of a laser, a telescope, an optical receiver, and detectors. Indoor CO_2 cell measurements show that the accuracy of the Raman lidar is 99.89%. Field measurements were carried out over a four-day period in November 2017 at the Eumsong Environmental Impact Evaluation Test Facility (EIT), Korea, where a CO_2 leak was located 0.2 km from the Raman lidar. The results show good agreement between CO_2 VMR measured by the Raman lidar system (CO_2 $VMR_{Raman\ LIDAR}$) and that measured by in situ instruments (CO_2 $VMR_{In\text{-}situ}$). The correlation coefficient (R), mean absolute error (MAE), root mean square error (RMSE), and percentage difference between CO_2 $VMR_{In\text{-}situ}$ and CO_2 $VMR_{Raman\ LIDAR}$ are 0.81, 0.27%, 0.37%, and 4.92%, respectively. The results indicate that Raman lidar is an effective tool in detecting CO_2 leakage and in measuring CO_2 VMR remotely.

Keywords: CO_2; Raman lidar; Carbon capture and storage; CO_2 leakage remote sensing

1. Introduction

The average temperature of Earth has increased by 0.8 °C since the beginning of the twentieth century, garnering worldwide interest [1]. This global warming is reported to be caused by an increase in the concentrations of greenhouse gases (e.g., CO_2, CH_4, N_2O, O_3, and CFCs) produced by human activities such as fossil fuel combustion, industrial processes, and deforestation [2,3].

As concern about increasing greenhouse gas concentrations has increased, many countries have begun to regulate carbon emissions [4] according to the Kyoto Protocol [5]. Carbon capture and storage (CCS) is considered a promising technology to reduce atmospheric CO_2 [3,6]. However, leakage of CO_2 from large-scale CCS can affect the CO_2 reduction efficiency and have serious impacts on the surrounding ecosystem, such as reduced soil pH, damage to plant and microbial communities, and groundwater contamination [7]. Previous studies [8,9] have monitored CO_2 leaking from CCS sites. Hui et al. [8] assessed CO_2 leakage from a storage facility in Xuzhou city, Jiangsu province, China, using multiple in situ instruments and wireless sensor networks. Elio et al. [9] reported a technique

for measuring CO_2 soil flux at an artificial CO_2 injection site in Hontomin, Spain. While these in situ instruments have a high CO_2 measurement accuracy, many instruments are required to monitor large CCS sites. It may be difficult to detect a small, continuous CO_2 leak if in situ instruments are sparsely distributed at a large CCS site. In contrast, remote sensing techniques can be used to monitor CO_2 leakages over a large CCS site using a single instrument. However, in compiling a map of CO_2 distribution via two-dimensional horizontal scanning, some spots might be missed by Raman lidar because of the nature of the terrain or the presence of obstacles.

The detection limit (LDL), accuracy, and cost of the in situ instrument used by Jung et al. [10] were 0 ppm, 1.5% of reading, and about \$35,000, respectively, while those of the instrument used by Jun et al. [11] were 0 ppm, 1% of reading, and about \$5500, respectively. There is no commercially available Raman lidar designed to measure CO_2. Only one previous study [12] has reported tropospheric CO_2 measurement using Raman lidar, although the authors provided no information on the LDL, precision, or cost of the lidar. Atmospheric CO_2 measurements have been reported down to 40 ppmv for 20,000 shots at altitudes up to 1.5 km. Since a lidar system with a 50 mJ laser and repetition rate of 20 Hz costs about \$40,000 [12], the cost of the lidar is thought to be higher than this figure.

In the present study, we developed a Raman lidar technique capable of detecting and remotely sensing the mixing ratio information of CO_2 leakage from the surface. The remainder of this paper is organized as follows. The Raman lidar hardware system and the algorithms used to retrieve the CO_2 volume mixing ratio (CO_2 VMR) are described in Section 2, and the indoor and outdoor CO_2 measurement performance of the system is reported in Sections 2 and 3. Finally, the discussion, and conclusions are given in Sections 4 and 5, respectively.

2. Materials and Methods

We used the elastic scattering and the Raman lidar equation to retrieve CO_2 mixing ratios. The lidar equation applied to CO_2 Raman lidar is as follows [13]:

$$\mathrm{P}(\lambda, z) = E(\lambda) \times \exp\left(-\int_0^z \alpha(\lambda, z)\mathrm{d}z'\right) \times \beta(\lambda, z) \times \exp\left(-\int_0^z \alpha(\lambda, z)\mathrm{d}z'\right) \frac{S_{area}}{z^2} \times \xi(z) \times \eta_\lambda, \quad (1)$$

where $\mathrm{P}(\lambda, z)$ is the returned backscatter signal from distance z at the laser wavelength λ, $E(\lambda)$ is the initial laser energy, α is the total (=aerosol + molecular) extinction coefficient, β is the total (=aerosol + molecular) backscatter coefficient, S_{area} is the telescope receiver area, ξ describes the overlap function, and η_λ is the receiver efficiency that reflects how many of the incoming photons are detected. Raman scattering refers to a process of inelastic scattering of light by molecules such as CO_2 in which the wavelength of the incident light is changed [14]. The Nd:YAG laser of wavelength 355 nm used in this study is shifted to a wavelength of 371.6 nm caused by the vibrational Raman process of CO_2 molecules. For reference, the Raman scattering wavelength of N_2 molecules in dry air in the lower troposphere is 386.7 nm. By using Equation (1), the backscattered signal from a Raman CO_2 channel at 371.6 nm, P_{CO_2}, can be expressed as

$$P_{CO_2}(z) = \frac{k_{CO_2}}{z^2}\sigma_{CO_2}(\pi)n_{CO_2}(z)q(\lambda_{CO_2}, z_0, z)\exp\left(-\int_0^z \alpha(\lambda, z)\mathrm{d}z'\right), \quad (2)$$

where k_{CO_2} is a proportionality constant for the system optical efficiency, the telescope receiver area, photomultiplier tube (PMT) efficiency, and the laser output energy. σ_{CO_2} is the backscattered cross-section for CO_2 caused by Raman scattering, n_{CO_2} is the number density for CO_2 as a function of distance z, and $\alpha(\lambda)$ is the volume extinction coefficient at wavelength λ.

$$P_{N_2}(z) = \frac{k_{N_2}}{z^2}\sigma_{N_2}(\pi)n_{N_2}(z)q(\lambda_{N_2}, z_0, z)\exp\left(-\int_0^z \alpha(\lambda, z)\mathrm{d}z'\right), \quad (3)$$

where k_{N_2} is a proportionality constant for the system optical efficiency, the telescope receiver area, photomultiplier tube (PMT) efficiency, and the laser output energy. σ_{N_2} is the backscattered cross-section for N_2 caused by Raman scattering, n_{N_2} is the number density for N_2 as a function of distance z, and $\alpha(\lambda)$ is the volume extinction coefficient at wavelength λ.

$$\exp\left(-\int_0^z \alpha(\lambda, z)dz'\right) = q(\lambda_0, z_0, z), \tag{4}$$

where $q(\lambda_0, z_0, z)$ is the atmospheric transmittance from Raman lidar at distance z_0 to z at wavelength 355 nm. We used Raman signals of N_2 as a reference to calculate the CO_2 mixing ratio. The CO_2 mixing ratio is the mass of CO_2 divided by the mass of dry air in a given volume [12]. Since N_2 is present at a constant rate in dry air, the N_2 Raman signal, P_{N_2}, is used as a measure of dry air [13]. The CO_2 mixing ratio can be derived from the normalization signal, which is the quotient of the CO_2 Raman signal divided by the N_2 Raman signal. The normalization signal can be expressed as

$$\text{Normalization signal} = \frac{P_{CO_2}(z)}{P_{N_2}(z)}. \tag{5}$$

The backscatter signals of CO_2 and N_2 were used to calculate the normalization signal. The Raman scattering signals of CO_2 and N_2 are obtained at different wavelengths (371.7 and 386.7 nm, respectively), and thus it has been assumed that there is no wavelength dependence with respect to extinction and consequently to atmospheric transmittance.

Figure 1 shows a flow chart of the process used to calculate the CO_2 volume mixing ratio using the Raman lidar system. First, the normalized ratio is calculated using the CO_2 and N_2 inelastic signals caused by Raman scattering, as measured by the Raman lidar system.

In the right part of Figure 1, the regression coefficients are determined using the calculated normalized ratio and the CO_2 VMR measured by the in situ instrument. The regression coefficients are then used in the calibration equation. The surface CO_2 mixing ratios are calculated using a regression between the calculated normalized ratio and the CO_2 VMR measured by an in situ instrument.
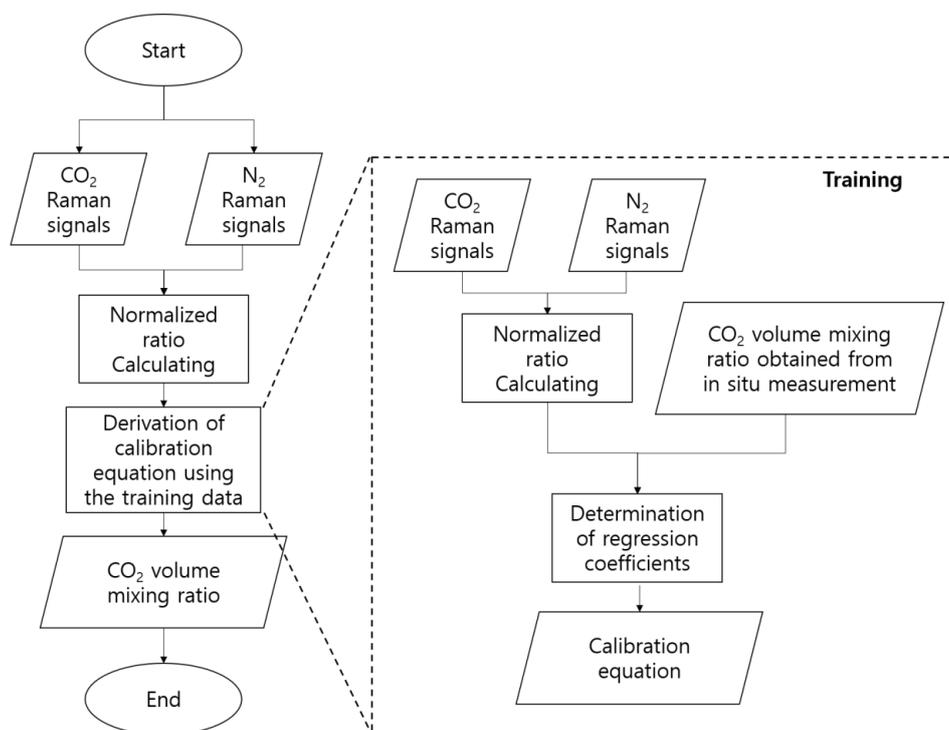

Figure 1. Flow chart for calculating the CO_2 volume mixing ratio using the Raman lidar system.

2.1. Raman Lidar Setup

The Raman lidar system consists of the third harmonic of a Nd:YAG laser of wavelength 355 nm with 80 mJ energy and 20 Hz repetition rate, a telescope, an optical receiver, and detectors. The pulsed laser is emitted horizontally to the ground from the Nd:YAG laser. Since the laser is emitted horizontally, the diameter of the laser beam was expanded, using a beam expander, by a factor of five times to ensure eye safety. The eye safety distance of our Raman lidar system is 208 m. The Raman lidar is applied co-axially with respect to the optical system to detect CO_2 near the location of the lidar, with an overlap distance of 5–10 m. To observe CO_2 mixing ratios, the Raman lidar system measures backscatter signals caused by CO_2 Raman, N_2 Raman, and Rayleigh–Mie scattering. These signals are detected and recorded as a function of distance and wavelength. To achieve real-time monitoring, a three-channel signal collection system was designed to collect the three types of backscatter signals simultaneously (Figure 2).
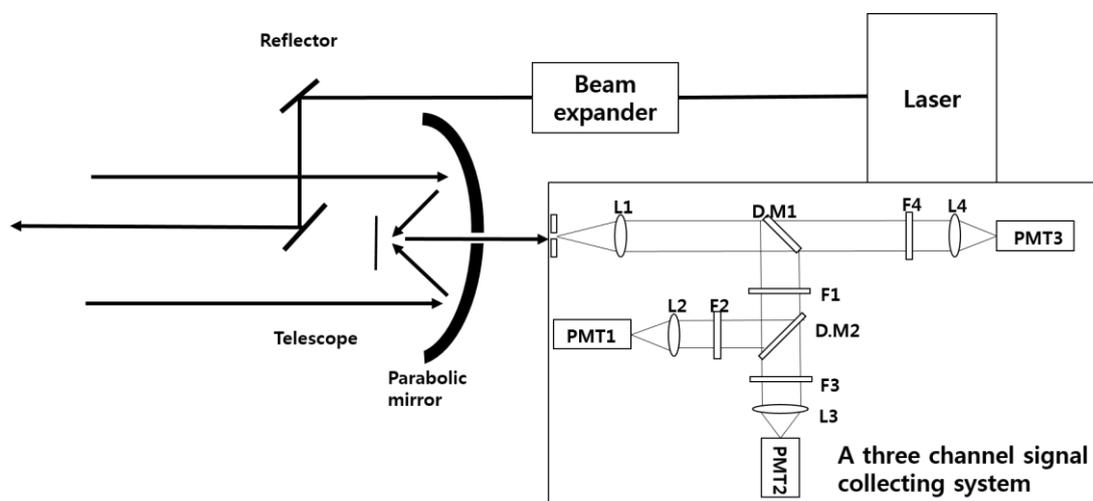

Figure 2. Schematic of the CO_2 Raman lidar system.

A Schmidt–Cassegrain telescope with a diameter of 15.24 cm is used as an optical receiver. First, the scattered light is collected by the telescope. After passing through a pinhole, it is narrowed by the collimating lens (L1). A dichroic beam splitter (D.M1) reflects the light at wavelengths above 355 nm. Since the Raman scattering signal is weaker than Rayleigh–Mie scattering [12], a notch filter (F1) is used which reflects light at 355 nm and transmits it at all other wavelengths, thus reflecting the elastic signals caused by Rayleigh–Mie (total) scattering and detecting the inelastic signal caused by Raman scattering. The CO_2 filter (F2) transmits light with a wavelength of 371.7 nm to detect the Raman scattering signals of CO_2 and reflects light at all other wavelengths. The CO_2 filter (F3) transmits light at 386.7 nm and reflects all other wavelengths to detect the Raman scattering signals of N_2 needed to calculate the CO_2 VMR. The 355 nm filter (F4) transmits light at 355 nm to detect the elastic scattering signal used in aligning the lidar signal. The lenses L2, L3 and L4 are used to focus the CO_2 Raman, N_2 Raman, and elastic signals into the PMT. The signals detected by the three-channel collecting system are analyzed to determine the CO_2 mixing ratio. Table 1 summarizes the main components of the CO_2 Raman lidar system.

Table 1. Components of the Raman lidar system.

Component	Specification
Laser	Nd:YAG laser Wavelength: 355 nm Pulse Energy: 80 mJ Beam divergence: <1.5 mrad (full angle) Repetition rate: 20 Hz Pulse duration: 9 ns
F1	Notch filter, 355 nm Spectral Range: 350–1100 nm Nominal Transmission: 1.0%
F2	CO_2 Raman (371.7 nm) CWL: 371.7 nm FWHM: 0.5 nm Tabs > 70% @ 371.7 nm (Typical T > 85%) OD > 7 @ 354.7 nm OD > 6 from 200–1200 nm out-of-band
F3	N_2 Raman (386.7 nm) FWHM < 0.6 nm OD7 Transmission: 386.7 nm > 80% T Absolute
F4	355 nm filter CWL: 355 nm FWHM: 10 nm OD > 5 Transmission > 90%
PMT1	CO_2 Channel R9880U-210
PMT2	N_2 Channel R9880U-210
PMT3	355 nm Channel R9880U-210
Telescope	6-In. Schmidt Cassegrain
Beam expander	5X, fixed beam-expander
Size of the Raman lidar system	$1100 \times 850 \times 550$ mm (W $\times$ H $\times$ D)
Weight of the Raman lidar system	70 kg
Power demand of the Raman lidar system	1000 W

2.2. Indoor CO_2 Cell Measurement

Indoor CO_2 cell measurements were carried out to quantify the accuracy of the lower detection limit of the Raman Lidar system. Figure 3 shows a schematic diagram of the indoor CO_2 cell setup using the Raman lidar. The cell measurement setup consists of a CO_2 gas vessel, a mass flow controller (MFC), a CO_2 gas cell, a vacuum pump, and the Raman lidar system. CO_2 in the CO_2 gas vessel is injected into the CO_2 cell using the MFC, which controls the CO_2 mixing ratio in the cell. A vacuum pump is connected to the cell to release CO_2 gas from the cell into the air.

To measure the VMR of CO_2 gas using Raman lidar, the inside of the CO_2 cell is evacuated and CO_2 gas is injected. The CO_2 VMR of the cell is set to range from 10% to 100%, as the lowest measurement unit of the vacuum gauge used in this study is 1%. The inelastic signals of CO_2 and N_2 caused by Raman scattering are subsequently measured by the Raman lidar and are hereafter referred to as the normalized ratio.
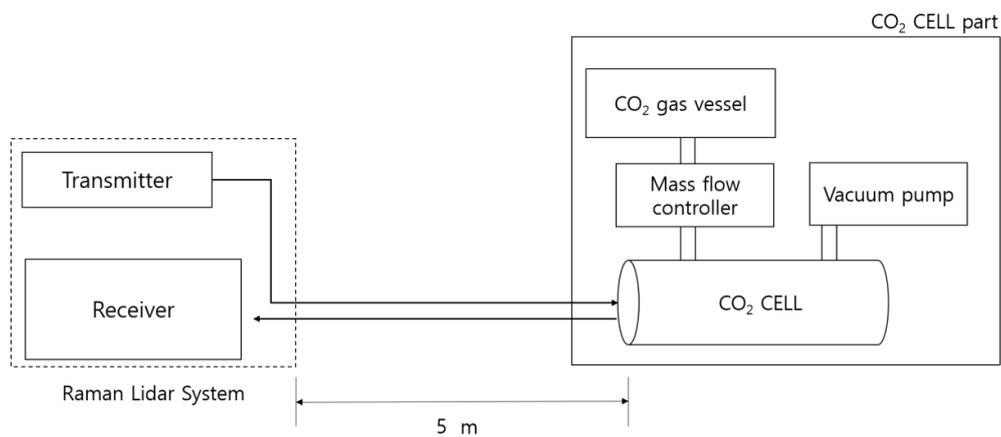
Figure 3. Schematic diagram of the indoor CO_2 cell test.

3. Results

3.1. Indoor CO_2 Cell Measurement

Figure 4 shows the correlation between the normalized ratio measured by CO_2 Raman lidar and the CO_2 VMRs from the CO_2 cell. The x-axis represents the CO_2 VMR inside the CO_2 cell (CO_2 VMR_{CELL}) and the y-axis represents the normalized ratio, calculated from the inelastic signals of CO_2 and N_2 caused by Raman scattering (see Equation (5)). The correlation coefficient (R) between the CO_2 $VMR_{Raman\ LIDAR}$ and the normalized ratio is 1, showing excellent agreement. The deviation from the regression line observed at CO_2 VMR of 10% in Figure 4 is due to the inaccuracy of the vacuum gauge used to set the CO_2 concentration in the vacuum cell. The vacuum gauge has a concentration error of 1%. Next, the CO_2 VMR in the cell is retrieved using the normalized ratio and the regression equation obtained in Figure 4 based on the method displayed in Figure 1.
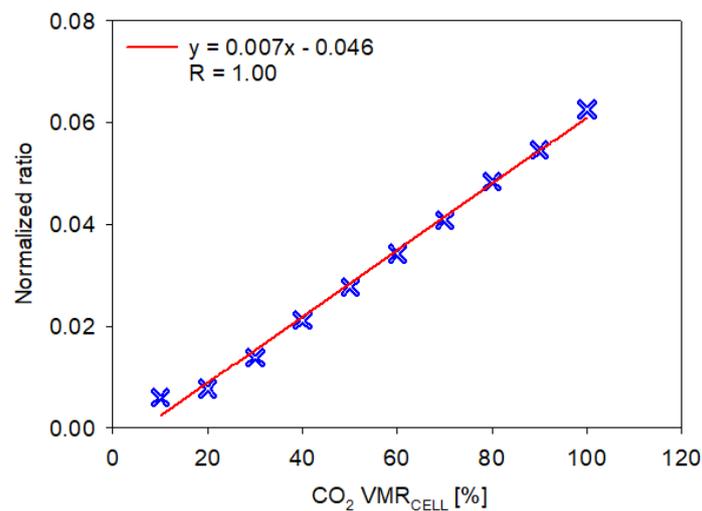

Figure 4. CO_2 VMR_{CELL} versus normalized ratio diagram.

Figure 5 shows the correlation between CO_2 VMR_{CELL} and CO_2 VMR as measured by the Raman lidar system (CO_2 $VMR_{Raman\ LIDAR}$). CO_2 $VMR_{Raman\ LIDAR}$ obtained from CO_2 Raman Lidar shows a good agreement with CO_2 VMR_{CELL}. Both R and the slope between CO_2 VMR_{CELL} and CO_2 $VMR_{Raman\ LIDAR}$ are 1.00. An R value close to 1 indicates more stable and consistent laser power and higher repeatability of the detector than an R value lower than 1, because CO_2 is the only variable that changes during the training and retrieval of indoor cell measurements of CO_2. If the R value departs from 1, then the output power of the laser is not consistent or the repeatability of the detector is not

sufficient for CO_2 retrieval. The CO_2 in the cell was measured 20 times by Raman lidar under constant conditions. We calculated the error of the value measured by Raman lidar when the CO_2 VMR in the cell was the same as that during CO_2 measurements. The CO_2 measurement accuracy of our Raman lidar is 99.89% based on the indoor CO_2 cell test.
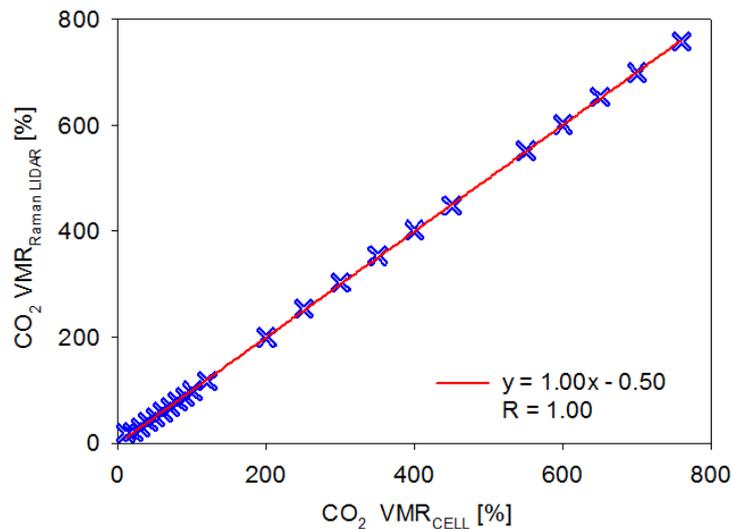

Figure 5. CO_2 VMR$_{CELL}$ versus CO_2 VMR$_{Raman\ LIDAR}$ diagram.

3.2. Field Test

To examine the Raman lidar system's capability in measuring spatially resolved CO_2 and N_2 Raman signals remotely, it was used to detect signals at a distance of 900 m from the lidar. The test was carried out on 30 October 2017, at a study site in Daejeon, South Korea, as shown in Figure 6a. We detected the Raman signals of CO_2 and N_2 for 1 h during the night. The effective spatial resolution of the Raman lidar was 250 ns (37.5 m). CO_2 and N_2 inelastic signals caused by Raman scattering were measured between the lidar system and a mountain location. During the daytime, the background signal from sunlight is stronger than the Raman scattering signal, so measurements were made only at night. Figure 6b shows the Raman signals of CO_2 and N_2 as a function of distance from the lidar system and the motorway. The increased CO_2 Raman signals found at 400 and 750 m from the lidar system represent the locations of a local motorway (A) and the Gapcheondosi Expressway (B), respectively. The enhanced Raman signals of CO_2 at locations A and B in Figure 6b imply that the lidar system is capable of detecting spatially resolved Raman signals of CO_2 emitted from motor vehicles. The Raman lidar obtained clear and stable Raman scattering signals of N_2 and CO_2 at a distance of 900 m from the lidar system.
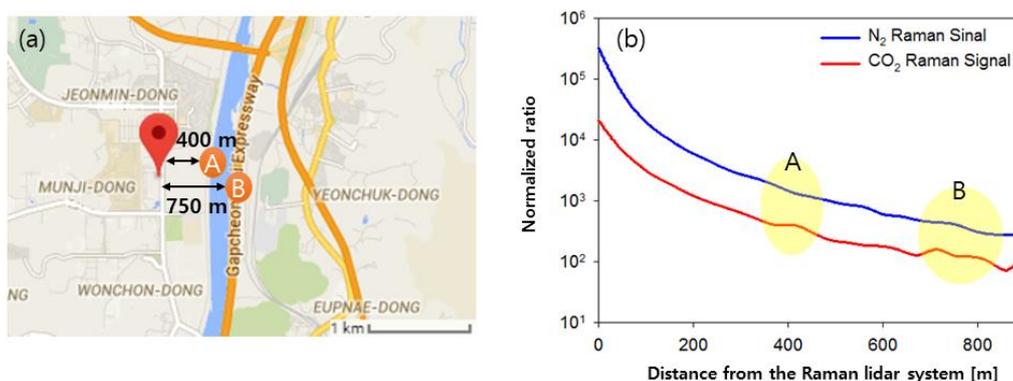

Figure 6. (**a**) Study area in Daejeon, Korea; (**b**) N_2 and CO_2 Raman signals measured by the Raman lidar system.

CO$_2$-Leakage Measurement Campaign

To examine the CO$_2$-leakage measurement capability of the lidar system, measurements were carried out using both the CO$_2$ Raman lidar system and an in situ CO$_2$ probe (VAISALA, GMP343). The measurements took place between 20 and 24 November 2017, at the Eumseong Environmental Impact Evaluation Test Facility (EIT) on Seepage of Geologically Stored CO$_2$, an artificial CO$_2$ gas-leakage site (36°96′N, 127°47′E). As shown in Figure 7, CO$_2$ is injected at 0.5 m below the surface and left to leak back out. CO$_2$ gas was injected into the ground at 12 L/min for 12 h on 22 November, 2017. The Raman lidar system is located 200 m from the in situ CO$_2$ measurement device, which is located near the CO$_2$ injection location. The Raman lidar line-of-sight is located 0.5 m above the surface of the CO$_2$ injection inlet. The effective spatial resolution of the Raman lidar is 250 ns (37.5 m) and the beam diameter is about 29.98 cm at the target. The in situ instrument measured the CO$_2$ VMR at a distance of 1 m from the Raman lidar line-of-sight. A linear regression equation between the normalized ratio and CO$_2$ VMR measured by the in situ instrument is derived based on the measurements on 24 November, 2017. Six hours after stopping the CO$_2$ gas injection, the measurement of CO$_2$ on the surface was started using the CO$_2$ Raman lidar. The change in Raman scattering signals with respect to the change in the CO$_2$ mixing ratio on the surface was measured as CO$_2$ gas was being injected into the ground at 12 L/min. During the campaign period, the in situ instrument with its inlet located 0.5 m from the surface often failed to measure CO$_2$ leakage near the surface. This is thought to be associated with low CO$_2$ concentrations even at 0.5 m from the surface, probably due to a negligible exit velocity of CO$_2$ molecules. To evaluate the performance via comparison with the in situ measurement, the point of view of the lidar system was focused at the in situ inlet location to increase the lidar's sensitivity to CO$_2$ molecules.
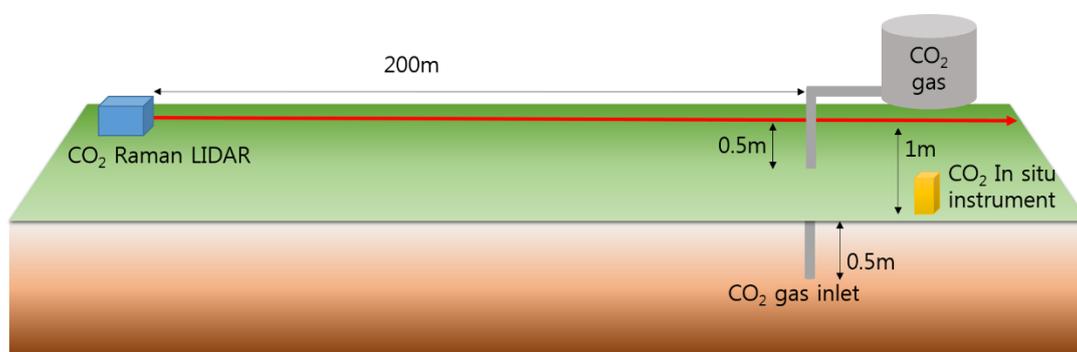

Figure 7. Schematic representation of the Eumseong Environmental Impact Evaluation Test Facility for the seepage of geologically stored CO$_2$.

Figure 8 shows the time series of CO$_2$ VMR$_{In-situ}$ measured by the in situ instrument (blue line) and CO$_2$ VMR$_{Raman\ LIDAR}$ measured by the Raman lidar system (red lines) at the Eumseong EIT site during the field campaign. The CO$_2$ gas was artificially injected into the ground and left to leak from the surface. An increasing trend in both CO$_2$ VMR$_{In-situ}$ and CO$_2$ VMR$_{Raman\ LIDAR}$ is expected with continued CO$_2$ injection. In Figure 8, the CO$_2$ VMR measured by the CO$_2$ Raman lidar increases steadily over time, while the CO$_2$ VMR measured by the in situ instrument shows an increasing trend with large variability over a short time interval. The reason for this difference between the steadily increasing CO$_2$ VMR$_{Raman\ LIDAR}$ and the increasing CO$_2$ VMR$_{In-situ}$ trend with large fluctuations could be associated with differences in measurement coverage. The spatial effective resolution of the Raman lidar is 37.5 m, which is different from the in situ instrument inlet area with a diameter of 1.5 cm. It is clearly shown that CO$_2$ VMR$_{Raman\ LIDAR}$ tends to be lower than CO$_2$ VMR$_{In-situ}$ obtained from the CO$_2$ leakage spot in Figure 9, which implies a certain influence of the ambient CO$_2$ VMR on the CO$_2$ VMR$_{Raman\ LIDAR}$ since the ambient CO$_2$ VMR is likely to be lower than the CO$_2$ VMR of the leakage and also does not change rapidly for a short time period [15]. In the present study, if the CO$_2$

concentration of the leak is lower than the concentration of CO_2 leaking from the field campaign in the case of a small leak, our current Raman lidar system with a spatial resolution of 37.5 m is barely able to detect the CO_2 leak due to the long spatial resolution of the system. Therefore, the spatial resolution of the lidar system is an important factor in improving the CO_2 precision and detection limit, especially for small leaks. A high-speed photon counter, which provides fine spatial resolution, is required to enhance the precision and detection limit. The LDL and precision of the Raman lidar are also thought to affect the overall efficiency and capability of the lidar to detect such small variations in low CO_2 levels. The trend difference in Figure 8 between CO_2 $VMR_{In-situ}$ and CO_2 $VMR_{Raman\ LIDAR}$ under windy conditions could be associated with the wind direction between a CO_2 leak and the measurement location of each instrument, as the closest distance between the Raman lidar line-of-sight and the in situ instrument is 1 m. However, the effect of wind direction and speed could not be quantified due to the unavailability of wind data during the campaign period.
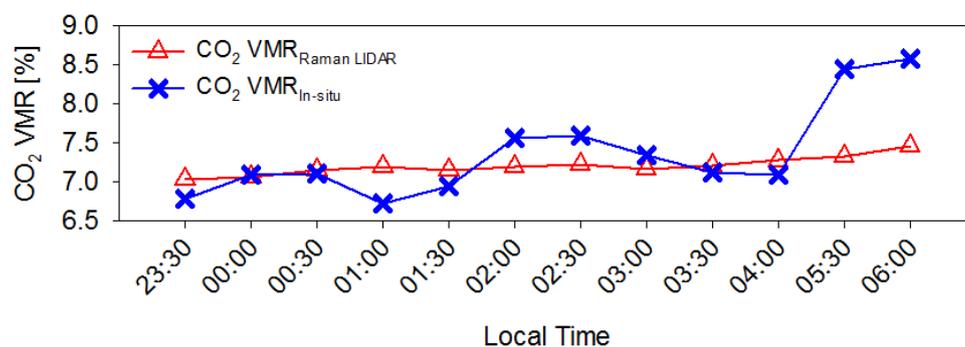

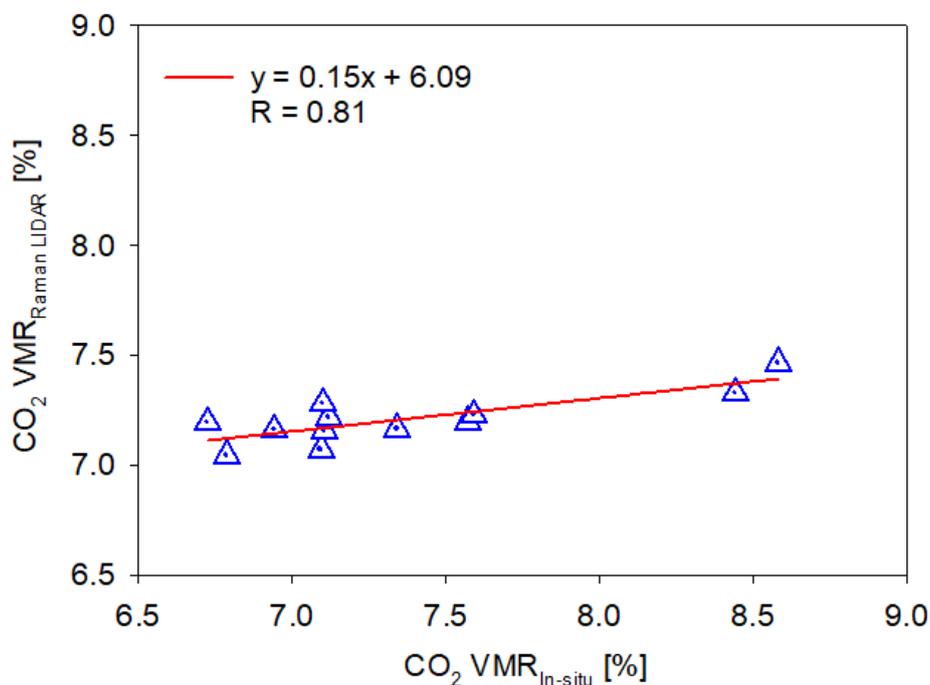**Figure 8.** Time series of CO_2 $VMR_{In-situ}$ and CO_2 $VMR_{Raman\ LIDAR}$ on November 23, 2017.

Figure 9. CO_2 $VMR_{In-situ}$ versus CO_2 $VMR_{Raman\ LIDAR}$ diagram.

Figure 9 shows the results of linear regression for CO_2 $VMR_{In-situ}$ and CO_2 $VMR_{Raman\ LIDAR}$ at the Eumseong EIT site, revealing a correlation. The R value and slope between CO_2 $VMR_{In-situ}$ and CO_2 $VMR_{Raman\ LIDAR}$ are 0.81 and 0.15, respectively. The mean absolute error (MAE), the root mean square error (RMSE) and the percentage difference between CO_2 $VMR_{In-situ}$ and CO_2 $VMR_{Raman\ LIDAR}$

are 0.27%, 0.37%, and 4.92%, respectively. The errors due to a decrease in backscattered Raman signals that follow a Poisson distribution are 4.9% (112.5 m), 5.4% (150.0 m), or 6.3% (187.5 m). The uncertainty due to the regression coefficients, as calculated from the residuals between the regression line and measured values, is 5.5%. Thus, the total error in CO_2 $VMR_{Raman\ LIDAR}$, which is calculated by error propagation, is estimated to be 7.4% (112.5 m), 7.7% (150.0 m), or 8.4% (187.5 m).

4. Discussion

Hui et al. [8] monitored CO_2 leakage from a geological CO_2 storage site in Xuzhou, Jiangsu, China, using multiple in situ instruments and wireless sensor networks, and Elio et al. [9] applied a technique for measuring CO_2 soil flux at a CO_2 injection site at Hontomin, Spain. While these in situ instruments have high CO_2 measurement accuracy, a large number of such instruments are needed to monitor large CCS sites. To enhance monitoring efficiency over a large area, remote sensing techniques are desired. Therefore, as part of efforts to develop remote sensing techniques for CO_2 measurements at the Earth's surface, we developed the first compact, lightweight, and portable Raman lidar system for remote sensing of surface CO_2 leakage. To examine the performance of the lidar, it was used to detect strong Raman signals of CO_2 at two roads located 400 and 750 m from the instrument. In the case of measurements at an artificial CO_2 leakage site, the CO_2 VMRs at 0.5 m from the surface and 200 m from the Raman lidar were measured successfully and show a good correlation with data collected by an in situ instrument. It is also necessary to understand the longest remote sensing distance with the highest possible accuracy. In order to quantify the longest remote sensing distance of our Raman lidar system, it should be measured in the area without any obstacles on the line of sight. To obtain a relative accuracy from the comparison between CO_2 VMRs obtained from in situ instrument and the lidar, multiple in situ sensors need to be deployed at several distances on the line of the lidar sight.

During the campaign period, the CO_2 VMRs were detected successfully only near the surface, probably due to the low CO_2 exit velocity from the ground. In the case of such low velocities, the altitude of the lidar line of sight needs to be lowered to measure CO_2, since this compound is likely to exist near the surface. However, lowering the measurement altitude may cause noise such as fluorescence effect in the backscatter signals if the laser encounters obstacles near the surface or the ground itself, arising from the lowered altitude of the line of sight. Our current CO_2 retrieval algorithm needs to be improved to account for fluorescence effects. In addition, Elio et al. [9] proposed a CCS area of 3 km $\times$ 3 km that requires a Raman lidar scan that can provide sufficiently high spatial resolution to detect CO_2 leakage from a small site. In the present study, a laser with 80 mJ power was used in the lidar. A laser with stronger power and a more efficient receiver is needed to generate the Raman signal of CO_2 for sites far from the laser and to detect weak CO_2 Raman signals. In addition, in the case of elevated terrain along the lidar line of sight, the measurement distance on the line of sight is reduced, meaning that a lidar located at a single spot cannot complete two-dimensional horizontal scanning over a large CCS site with elevated terrain.

5. Conclusions

We developed a Raman lidar system that remotely detects CO_2 leakage and CO_2 VMR. The system consists of a laser, a telescope, an optical receiver, and detectors. In terms of indoor CO_2 cell measurement, CO_2 Raman lidar shows very high accuracy. Field measurements were carried out using Raman lider at the Eumseong EIT site where a CO_2 leak is located 0.2 km from the Raman lidar system. There is good agreement between CO_2 $VMR_{Raman\ LIDAR}$ as measured by the Raman lidar system and CO_2 $VMR_{In-situ}$ as measured by an in situ instrument at the Eumseong EIT site. The R value and percentage difference between CO_2 $VMR_{In-situ}$ and CO_2 $VMR_{Raman\ LIDAR}$ are 0.81 and 4.92%, respectively. Discrepancies between the CO_2 values measured by Raman lidar and by the in situ instrument could be due to differences between measurement coverage and the measurement geometry of the two approaches. In the case of low CO_2 exit velocities, it is necessary to measure the CO_2 by lowering the altitude of both lidar and in situ instruments. In the case of lidar, lowering the

measurement altitude may cause noise signals such as fluorescence to be included in the backscatter signals when the laser hits the ground due to the terrain. Therefore, the lidar algorithm and measurement methods need to be studied further. The CO_2 VMR measurement resolution and detection limit also requires further study at low levels of CO_2. In a future experiment, wind data will be used to assess the optimal measurement height for the detection and measurement of CO_2 leaks.

Author Contributions: The Raman lidar system was developed by H.K., S.C., S.P., and M.Y. In situ data collection and analysis were done by S.-T.Y. and S.-C.J. Retrieval of CO_2 $VMR_{Raman\ LIDAR}$ was conducted by D.K., H.L. and J.-Y.R.

References

1. Ko, D.; Yoo, G.; Yun, S.T.; Chung, H. Impacts of CO_2 leakage on plants and microorganisms: A review of results from CO_2 release experiments and storage sites. *Greenh. Gas. Sci. Technol.* **2016**, *6*, 319–338. [CrossRef]

2. Metz, B. (Ed.) *Carbon Dioxide Capture and Storage: Special Report of the Intergovernmental Panel on Climate Change*; Cambridge University Press: Cambridge, UK, 2005.

3. IPCC. *Climate Change 2014: Mitigation of Climate Change. Contribution of Working Group III to the Fifth Assessment Report of the Intergovernmental Panel on Climate Change*; Edenhofer, O., Pichs-Madruga, R., Sokona, Y., Farahani, E., Kadner, S., Seyboth, K., Eds.; Cambridge University Press: Cambridge, UK; New York, NY, USA, 2014.

4. Andrews, A.E.; Kofler, J.D.; Trudeau, M.E.; Williams, J.C.; Neff, D.H.; Masarie, K.A.; Chao, D.Y.; Kitzis, D.R.; Novelli, P.C.; Zhao, C.L.; et al. CO_2, CO, and CH 4 measurements from tall towers in the NOAA Earth System Research Laboratory's Global Greenhouse Gas Reference Network: Instrumentation, uncertainty analysis, and recommendations for future high-accuracy greenhouse gas monitoring efforts. *Atmos. Meas. Tech.* **2014**, *7*, 647–687. [CrossRef]

5. Grubb, M.; Vrolijk, C.; Brack, D. *The Kyoto Protocol: A Guide and Assessment*; Royal Institute of International Affairs Energy and Environmental Programme: London, UK, 1997; ISBN 1853835803.

6. Koornneef, J.; Ramírez, A.; Turkenburg, W.; Faaij, A. The environmental impact and risk assessment of CO_2 capture, transport and storage–an evaluation of the knowledge base. *Prog. Energy Combust. Sci.* **2012**, *38*, 62–86. [CrossRef]

7. West, J.M.; Pearce, J.M.; Coombs, P.; Ford, J.R.; Scheib, C.; Colls, J.J.; Smith, K.L.; Steven, M.D. The impact of controlled injection of CO_2 on the soil ecosystem and chemistry of an English lowland pasture. *Energy Procedia* **2009**, *1*, 1863–1870. [CrossRef]

8. Yang, H.; Qin, Y.; Feng, G.; Ci, H. Online monitoring of geological CO_2 storage and leakage based on wireless sensor networks. *IEEE Sensors J.* **2013**, *13*, 556–562. [CrossRef]

9. Elío, J.; Nisi, B.; Ortega, M.F.; Mazadiego, L.F.; Vaselli, O.; Grandia, F. CO_2 soil flux baseline at the technological development plant for CO_2 injection at Hontomin (Burgos, Spain). *Int. J. Greenh. Gas Control* **2013**, *18*, 224–236. [CrossRef]

10. Jung, N.H.; Han, W.S.; Watson, Z.T.; Graham, J.P.; Kim, K.Y. Fault-controlled CO_2 leakage from natural reservoirs in the Colorado Plateau, East-Central Utah. *Earth Planet. Sci. Lett.* **2014**, *403*, 358–367. [CrossRef]

11. Jun, S.C.; Cheon, J.Y.; Yi, J.H.; Yun, S.T. Controlled release test facility to develop environmental monitoring techniques for geologically stored CO_2 in Korea. *Energy Procedia* **2017**, *114*, 3040–3051. [CrossRef]

12. Zhao, P.; Zhang, Y.; Wang, L.; Cao, K.; Su, J.; Hu, S.; Hu, H. Measurement of tropospheric CO_2 and aerosol extinction profiles with Raman lidar. *Chin. Opt. Lett.* **2008**, *6*, 157–160. [CrossRef]

13. Stoyanov, D.; Grigorov, I.; Kolarov, G.; Peshev, Z.; Dreischuh, T. LIDAR atmospheric sensing by metal vapor and Nd: YAG lasers. In *Advanced Photonic Sciences*; InTech: London, UK, 2012.

14. Whiteman, D.N.; Melfi, S.H.; Ferrare, R.A. Raman lidar system for the measurement of water vapor and aerosols in the Earth's atmosphere. *App. Opt.* **1992**, *31*, 3068–3082. [CrossRef] [PubMed]

15. Ehleringer, J.R.; Cerling, T.E. Atmospheric CO_2 and the ratio of intercellular to ambient CO_2 concentrations in plants. *Tree Physiol.* **1995**, *15*, 105–111. [CrossRef] [PubMed]